Journal of Computational Applied Mechanics 2022, 53(2): 244-263

DOI: 10.22059/JCAMECH.2022.338886.692

RESEARCH PAPER

Energy, exergy and economic analysis of an improved Kalina cycle integrated with a proton exchange membrane fuel cell

Armin Emamifar*

Department of Mechanical Engineering, Ayatollah Boroujerdi University, Boroujerd, Iran

Abstract

Integrating a PEM fuel cell with an improved Kalina cycle to gain more electrical power is presented in this study. The Kalina cycle consists of two turbines and two separators. The waste heat of the PEM fuel cell is the major energy source for the Kalina cycle and industrial waste heat is supplied to the cycle to generate more electrical energy. Thermodynamic and exergoeconomic analysis is carried out on the system components to evaluate the system performance. The results indicate that the proposed system can produce 14.51 % more power in comparison with the standalone PEM fuel cell, while the total cost rates of the system increase by 19.3 %. Moreover, the energy and exergy efficiencies of the proposed hybrid system is 5.01% and 14 % higher than the energy and exergy efficiencies of the standalone PEM fuel cell. The exergoeconomic analysis shows that the fuel cell, the turbines, the compressor and the condenser have the highest cost rates compared to other components of the system. Furthermore, a parametric study is performed on the system to investigate the effect of variations of some key parameters, including PEM fuel cell operating temperature and pressure, current density, ammonia mass fraction and maximum pressure of the Kalina cycle on system performance.

Keywords: PEM fuel cell; Kalina cycle; energy; exergy; exergoconomic analysis

1. Introduction

Reducing energy consumption, lowering the system costs, and enhancing the efficiency of the systems, have always been the main goals for thermal systems. In recent years, due to growing energy demand, depletion of fossil fuel resources, and increasing environmental problems, special attentions have been paid to the use of renewable and clean energies. In this regard, the use of waste energies to produce power, heat, and refrigeration has been one of the most considerable solutions. Combined heating and power (CHP) systems can save up to 40% in primary energy consumption [1-3]. However, employing renewable energies in CHP systems, can reduce environmental impacts, as well as system costs [4]. Development of new structures, technologies, systems, and energies have received much attention in recent years [5-37]. The PEM fuel cells have been a promising source of energy due to advantages such as low operating temperature, high power density, high efficiency, quick start-up, safety, and low environmental problems. The fuel uses in the PEM fuel cells is hydrogen which does not have limitations such as needing a special site and generation of chemical wastes. Moreover, PEM fuel cells produce electricity and heat with water as only by-product [38, 39]. The energy efficiency of a PEM fuel cell is in the range of 30% to 50% depending on its operating conditions. The rejected heat from the fuel cell to maintain its temperature is the main factor of inefficiency in this component. Utilization of waste heat from the PEM fuel cell in other thermal systems can enhance the energy efficiency of the system. PEM fuel cell is a low-temperature heat source and there are limitations and challenges for the type of systems that can be considered for recovering its waste heat [40]. Several

* Corresponding author: emamifar@abru.ac.ir

investigations have been carried out to study the ability of waste heat recovery from a PEM fuel cell to enhance the efficiency of the system in power, refrigeration, CHP, and CCHP systems. Malik et al. [41] proposed new CCHP systems employing PEM and thermoelectric generator in a Kalina cycle which uses geothermal water as source energy. Their results showed that the use of PEM and TEG in a Kalina based power cycle can improve the exergoeconomic performance of the conventional geothermal based Kalina cycle. Li et al. [42] employed a PEM fuel cell to improve the performance of a geothermal based organic Rankine flash cycle. Their results showed that using the waste heat of the PEM fuel cell instead of the low-temperature geothermal source can increase the energy efficiency from 4.94% to 23.6% and exergy efficiency from 23.77% to 36.19%. However, 9.07US$/h increment in cost rates was obtained by the proposed system. Sarabchi et al.[43] analyzed the thermo-economic and environmental performance of a new cogeneration system consisting of a high temperature PEM fuel cell, a Kalina cycle, and a solar methanol steam reformer. Compared to a standalone PEM fuel cell system, the proposed cogeneration system could achieve enhancements of up to 9.6% and 4.3% in the energy and exergy efficiencies. Ahmadi et al. [44] used the waste heat of a PEM fuel cell in a hybrid system consisting of a transcritical CO2 cycle and a LNG cycle to produce electricity and chilled water. The results showed 39.56% enhancement in the power generation compared to the standalone fuel cell system.. Seyed Mahmoudi et al. [45] used the waste heat of a PEMFC as a heat source for an organic Rankine cycle to produce electricity and presented the exergoeconomic analysis for the proposed system. They reported that total exergy efficiency can increase by 4.76% in comparison with the standalone PEM fuel cell. Rezaee and Houshmand [46] studied the performance of a combined Kalina and PEMFC system and reported that energy and exergy efficiencies can improve 1.75% and 1.5% compared to a standalone PEMFC system. Chahartaghi and Kharkeshi [47] employed a PEMFC as prime mover in a CCHP system consisting of an absorption system and a heat storage tank. The system was compared with the conventional energy systems for residential applications. The results showed that maximum exergy destruction occur in the PEM fuel cell. Zhao et al. [48] proposed a hybrid system in which an organic Rankine cycle used the waste heat of a proton exchange membrane fuel cell as energy source. Their thermodynamic analysis results showed that the efficiency of the hybrid system can increase by 5% compared to simple PEM fuel cell stack. Kaushik et al. [49] combined a PEMFC with regenerative organic Rankine cycle and analyzed the thermodynamic performance of the system. They also analyzed different models by varying the different parameters of the regenerative organic Rankine cycle as well as the PEM fuel cell. Toghyani et al. [50] used a PEMFC stack as a heat source for an ejector absorption refrigeration system and studied the effect of condenser pressure and generator temperature on the system performance. The results showed that the COP of absorption chiller with ejector at the operating temperature of 80 °C and the pressure of 1 bar for PEM fuel cell is 6.7% higher than conventional absorption chiller. Baniasadi et al. [51] proposed a hybrid system based on a PEMFC and an absorption system to produce electricity, space cooling and hot water for a residential application and demonstrated that operating temperature, operating pressure, and fuel cell voltage are important parameters for exergy costs of the system. Marandi et al. [52] employed a parallel two-stage organic Rankine cycle for utilizing the waste heat of a PEM fuel cell and hydrogen boil-off gas stream as a heat sink for the cycle., energy efficiency and exergy efficiency, and Exergoeconomic factor of the system were computed to be 36.64%, 58.15%, and, 26.21%, respectively. They also indicated that that the lower operating temperature and higher current density, will raise the total cost rate. Fakhari et al. [53] carried out the single and multi-objective optimization on a hybrid system consisting of a PEMFC and organic Rankin cycle for different zeotropic mixtures and introduced the best combination mixtures for achieving high efficiency.

The literature review shows that combination of PEM fuel cells with various thermal systems have been investigated. However, due to importance of employing low temperature energy, improving the hybrid systems in order to enhance energy, exergy and economic performance always need to be given more consideration. Among various power systems, the Kalina cycle is a considerable choice. The Kalina cycle uses ammonia/water mixture as working fluid which has advantages like availability, inexpensiveness, variable boiling temperature, being eco-friendly and compatibility with many standard materials [54-57]. In the present study, an improved configuration of a Kalina cycle is integrated with a PEM fuel cell and industrial waste heat to recover more electrical work. PEM fuel cell acts as prime energy source for the cycle. Unlike many previous studies, in this work, the energy of weak ammonia/water solution leaving the separator of the Kalina cycle is improved by industrial waste heat to produce more electrical energy through the second turbine placed in the Kalina cycle. Thermodynamic and Thermoeconomic analysis is performed on the proposed system to identify the benefits and disadvantages of the system. Furthermore, the effect of the capital parameters of the fuel cell and Kalina cycle on the efficiency and different costs of the system components is investigated. In summary, the followings are the main objectives and novelties of the present study:

- To propose a hybrid system for recovery the rejected heat from a PEM fuel cell.
- Employing low-temperature industrial waste heat to recovery more waste energy and produce more electrical work.

- Analyzing the system from energy, exergy and economic viewpoint.
- Investigation the important parameters of the PEM fuel cell and Kalina cycle on the thermodynamic and economic performance of the system.

2. System Description

The schematic diagram of the proposed system is shown in Fig.1. Hydrogen and air are supplied to the anode and cathode of the fuel cell, respectively. Hydrogen from H2 tank passing through a regulator valve and humidifier is fed to the anode of the fuel cell. Meanwhile, compressed air which is pressurized by compressor enters the cathode of the fuel cell. Then, electrochemical reaction occurs in the fuel cell to produce electrical work. The fuel cell outlets are water, air and hydrogen. To recycling utilization, the unreacted hydrogen is returned back to the inlet of the fuel cell. However, considerable amount of heat is also generated in this procedure that transfers to a double turbine Kalina cycle. The ammonia/water solution from the Kalina pump outlet passes through the HTR and enters the fuel cell to absorb waste heat of the fuel cell. Some liquid solution vaporizes by absorbing the waste heat of the fuel cell. The two-phase ammonia/water mixture is delivered to the separator I where the stream is separated into ammonia vapor and weak ammonia/water solution. The ammonia vapor enters the turbine I to produce power. The weak ammonia/water solution enters the heat exchanger (HEX) to absorb heat from a low grade source to form a two-phase mixture which is fed to the separator II. The strong ammonia vapor leaving the separator II enters the turbine II to generate additional power. The weak ammonia/water mixture leaving the separator II goes through the HTR, where it cools down. Afterwards, it passes through the expansion valve II, and enters the mixer. In the mixer, the outlet stream of the turbine I, turbine II, and HTR are mixed together to form the ammonia/water basic solution. Then, the ammonia/water basic solution is cooled down to saturated liquid in the condenser. Finally, the saturated ammonia/water solution pumps to the fuel cell to complete the cycle.

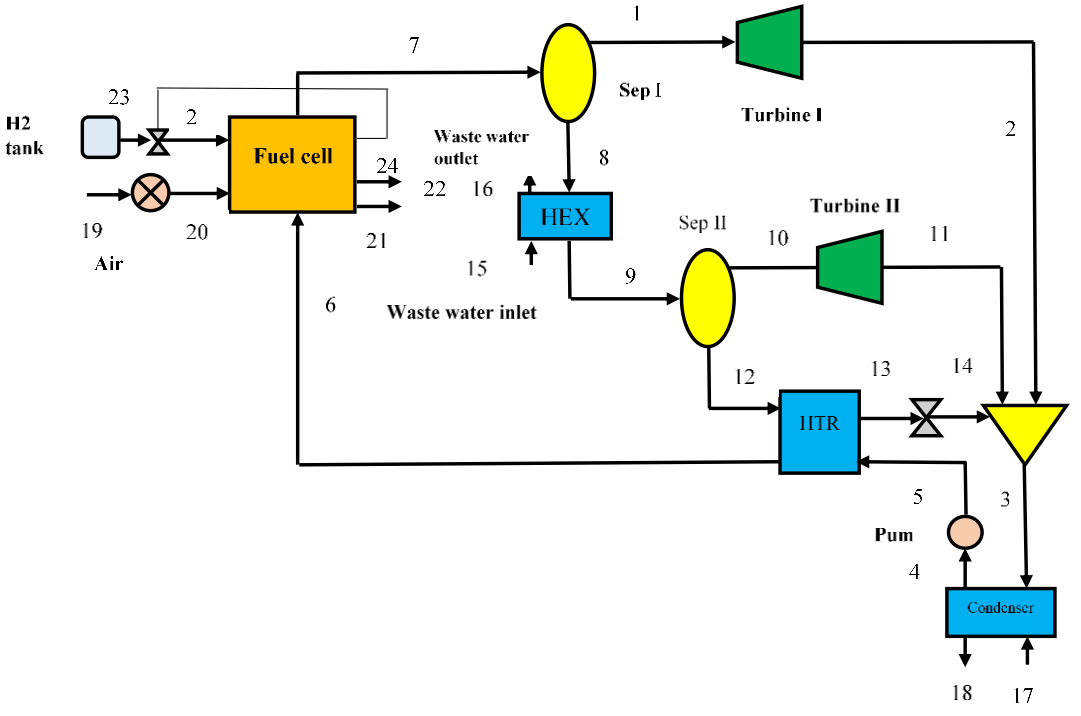

Fig. 1. The proposed Kalina cycle integrated with a PEM fuel cell

3. PEM fuel cell

In PEM fuel cells, hydrogen and air are fed into the electrodes to produce electricity, heat and water after electrochemical reactions. The electrical work produced through the reactions at the fuel cell can be calculated as follows [52]:

$$W_{fc} = N_{Cell} V_{fc} I \tag{1}$$

Where, N_{cell} is the number of cells in the stack, I is the current and V_{fc} is the actual voltage output of the cell. The actual voltage of the cell can be calculated from the Eq. (2) [52]:

$$V_{fc} = E_{Nernst} - V_{act} - V_{ohm} - V_{conc} \tag{2}$$

Where, E_{Nernst} is the open circuit voltage. Moreover, V_{act}, V_{ohm} and V_{conc} are the activation, ohmic and concentration over voltage, respectively. The open circuit voltage can be obtained from the well-known Nernst equation [48]:

$$E_{Nernst} = \frac{-\Delta G^0}{n_e F} + \frac{RT_{fc}}{n_e F} \ln\left(\frac{P_{H_2} \left(P_{O_2}\right)^{0.5}}{P_{H_2O}^{sat}} \right) \tag{3}$$

Where, ΔG^0 represents the Gibbs free energy, n_e is the number of electrons participating in the electrochemical reaction, F denotes the Faraday constant, R represents the universal constant of gas, T_{fc} is the fuel cell operating temperature, P_{H_2} and P_{O_2} represent the partial pressure of hydrogen and oxygen which are calculated as [48]:

$$P_{H_2} = \left(0.5 P_{H_2O}^{sat}\right) \left[\frac{1}{exp\left(1.653 i / T_{fc}^{1.334}\right).x_{H_2O}^{sat}} - 1 \right] \tag{4}$$

$$P_{O_2} = P\left[1 - x_{H_2O}^{sat} - x_{N_2}^{channel} exp\left(0.291 i / T_{fc}^{0.832}\right)\right] \tag{5}$$

Where P is the fuel cell operating pressure. The saturated pressure of water vapor ($P_{H_2O}^{sat}$) can be calculated using the following equation [52]:

$$\begin{aligned} &\log\left(P_{H_2O}^{sat}\right) = -2.1794 + 0.02953\left(T_{fc} - 273.15\right) \\ &-9.1837\times10^{-5}\left(T_{fc} - 273.15\right)^2 + 1.4454\times10^{-7}\left(T_{fc} - 273.15\right)^3 \end{aligned} \tag{6}$$

$x_{N_2}^{channel}$ and $x_{H_2O}^{sat}$ are the molar fraction of nitrogen and water in the gas flow at saturation for the specified temperature and, i is the current density [48].

$$x_{N_2}^{channel} = \frac{\left(x_{N_2,in} - x_{N_2,out}\right)}{\ln\left(\frac{x_{N_2,in}}{x_{N_2,out}} \right)} \tag{7}$$

$$x_{N_2,in} = 0.79\left(1 - x_{H_2O}^{sat}\right) \tag{8}$$

$$x_{N_2,out} = \frac{1 - x_{H_2O}^{sat}}{1 + \left(\left(\lambda_{air} - 1\right) / \lambda_{air}\right)\left(0.21 / 0.79\right)} \tag{9}$$

$$x_{H_2O}^{sat} = \frac{P_{H_2O}^{sat}}{P} \tag{10}$$

Where $x_{N_2,in}$ and $x_{N_2,out}$ denote the nitrogen molar fraction at inlet and outlet stream, respectively. Moreover, λ_{air} represents the stoichiometric rate of air. The activation overvoltage is calculated by the following semi-empirical relation: [52]:

$$V_{act} = -\left[-0.948 + \xi T_{fc} - 0.000193 T_{fc} \left(\ln\left(C_{O_2,conc}\right)\right) + 0.000076 T_{fc} \left(\ln(I)\right) \right] \tag{11}$$

$$\xi = 0.00286 + 0.0002 \ln\left(A_{cell}\right) + 0.000043 \ln\left(C_{H_2,conc}\right) \tag{12}$$

Here, A_{cell} is the surface area of the fuel cell, $C_{O_2,conc}$ represents the oxygen concentration at fuel cell cathode membrane interface, and $C_{H_2,conc}$ denotes the hydrogen concentration at fuel cell anode membrane interface. $C_{O_2,conc}$ and $C_{H_2,conc}$ can be obtained as follows [52]:

$$C_{O2,conc} = 1.97\times10^{-7} P_{O_2} \exp\left(\frac{498}{T_{fc}}\right) \tag{13}$$

$$C_{H_2,conc} = 9.174\times10^{-7} P_{H_2} \exp\left(\frac{-77}{T_{fc}}\right) \tag{14}$$

According to Ohm's law, the ohmic overvoltage can be expressed as [48]:

$$V_{ohm} = IR_{\text{int}} \tag{15}$$

$$R_{\text{int}} = \frac{r_{mem}L}{A_{cell}} \tag{16}$$

$$r_{mem} = \frac{181.6\left[1+0.03i+0.062\left(\frac{T_{fc}}{303}\right)^2 i^{2.5}\right]}{\left(\psi-0.634-3i\right)\exp\left(4.18\left(T_{fc}-303\right)/T_{fc}\right)} \tag{17}$$

where R_{int} represents the cell internal resistance, r_{mem} is the membrane resistivity, and ψ is the membrane water content. The concentration overvoltage which is due to variations in reactants concentration at the surface of the electrodes is given as [42]:

$$V_{conc} = \frac{RT_{fc}}{n_e F}\ln\left(\frac{i_L}{i_L - i}\right) \tag{18}$$

where i_L is the limiting current density. In order to calculate the produced waste heat by the fuel cell, the energy balance is written as follows:

$$\dot{Q}_{net} = \dot{Q}_{ch} - \dot{W}_{fc} - \dot{Q}_{s,l} \tag{19}$$

where $\dot{Q}_{net}$ represents the net produced heat by the fuel cell, $\dot{Q}_{ch}$ is the chemical energy and $\dot{Q}_{s,l}$ is the sensible and latent heat of inlet and outlet streams through the fuel cell. $\dot{Q}_{ch}$ is obtained from Eq.(22) [48]:

$$\dot{Q}_{ch} = \dot{n}_{H_2,cons} HHV \tag{20}$$

where $\dot{n}_{H_2,cons}$ is the consumption rate of hydrogen and is defined as [48]:

$$\dot{n}_{H_2,cons} = N_{cell}\frac{I}{2F} \tag{21}$$

The consumption rate of oxygen and the generation rate of water are calculated as follows [42]:

$$\dot{n}_{O_2,cons} = N_{cell}\frac{I}{4F} \tag{22}$$

$$\dot{n}_{H_2O,gen} = N_{cell}\frac{I}{2F} \tag{23}$$

Considering stoichiometric ratios of H_2 and O_2, the molar flow rate of the reactants are [42]:

$$\dot{n}_{H_2} = \lambda_{H_2} \dot{n}_{H_2,cons} = \lambda_{H_2} N_{cell} \frac{I}{2F} \tag{24}$$

$$\dot{n}_{O_2} = \lambda_{O_2} \dot{n}_{O_2,cons} = \lambda_{H_2} N_{cell} \frac{I}{4F} \tag{25}$$

Furthermore, the sensible heat and the latent heat are calculated employing the following equation [52]:

$$\dot{Q}_{s,l} = C_{p,H2}\left(\dot{n}_{H_2,out} T_{fc} - \dot{n}_{H_2,in} T_{in}\right) + C_{p,O_2}\left(\dot{n}_{O_2,out} T_{fc} - \dot{n}_{O_2,in} T_{in}\right) + C_{p,N_2}\left(\dot{n}_{N_2,out} T_{fc} - \dot{n}_{N_2,in} T_{in}\right) + \dot{n}_{H_2O,gen} H_v \tag{26}$$

where C_{p,H_2}, C_{p,O_2}, C_{p,N_2}, are the specific heat capacity of hydrogen, oxygen and nitrogen, respectively, H_v is the vaporization heat capacity of water.

The compressor work and the energy efficiency of the fuel cell can be expressed as [48]:

$$\dot{W}_{comp} = \frac{\dot{m}_{air}\left(k/(k-1)\right) RT_{amb}\left(\pi^{\left(\frac{k-1}{k}\right)} - 1\right)}{\left(\eta_{comp}\right)} \tag{27}$$

$$\eta_{fc} = \frac{\dot{W}_{fc} - \dot{W}_{comp}}{\left(\dot{n}_{H_2,cons}\right).HHV} \tag{28}$$

where k is the ratio of the air specific heat, π is the pressure ratio, η_{comp} is the compressor efficiency, and HHV is the higher heating value of the hydrogen.

4. Kalina double turbine cycle

To perform the thermodynamic analysis of the Kalina cycle, the following assumptions are considered:

-The system operates under steady state.

-The outlet stream of the condenser is saturated liquid.

-The outlet vapor and the outlet liquid streams from the separator are saturated vapor and saturated liquid, respectively.

-The pressure drop through the heat exchangers of the cycle is neglected.

-The isenthalpic process is occurred through the expansion valves.

-Industrial waste heat is considered as the source for the second turbine of the Kalina cycle.

In order to avoid overheating, the generated heat by the PEM fuel cell should be removed. In the present system, the waste heat of the fuel cell which is absorbed by the Kalina cycle can be expressed as:

$$\dot{Q}_{net} = \dot{m}_7\left(h_7 - h_6\right) \tag{29}$$

Moreover, the extra heat applied to the saturated liquid outlet of the separator I can be calculated as follows:

$$\dot{Q}_{HEX} = \dot{m}_w\left(h_{15} - h_{16}\right) = \dot{m}_8\left(h_9 - h_8\right) \tag{30}$$

The actual specific enthalpy for the outlet streams of turbine I, turbine II and pump are calculated using their isentropic efficiencies as follows:

$$\eta_{turI} = \frac{h_1 - h_2}{h_1 - h_{2s}} \tag{31}$$

$$\eta_{turII} = \frac{h_{10} - h_{11}}{h_{10} - h_{11s}} \tag{32}$$

$$\eta_{pump} = \frac{h_{5s} - h_4}{h_5 - h_4} \tag{33}$$

where η_{turI}, η_{turII} and η_{pump} are isentropic efficiencies of turbine I, turbine II and pump, respectively.

The power generated by turbine I and turbine II are obtained from Eq. (34) and Eq. (35) respectively.

Furthermore, the power consumption by pump can be calculated from Eq. (37):

$$\dot{W}_{turbineI} = \dot{m}_1 (h_1 - h_2) \quad (34)$$

$$\dot{W}_{turbineII} = \dot{m}_{10} (h_{10} - h_{11}) \quad (35)$$

$$\dot{W}_{turbine} = \dot{W}_{turbineI} + \dot{W}_{turbineII} \quad (36)$$

$$\dot{W}_{pump} = \dot{m}_5 (h_5 - h_4) \quad (37)$$

The heat rejection in the condenser is given by:

$$\dot{Q}_{cond} = \dot{m}_3 (h_3 - h_4) = \dot{m}_{cw} (h_{18} - h_{17}) \quad (38)$$

where $\dot{m}_{cw}$ is the mass flow rate of the cooling water in the condenser. The solution procedure of the system is presented in Fig. 2.

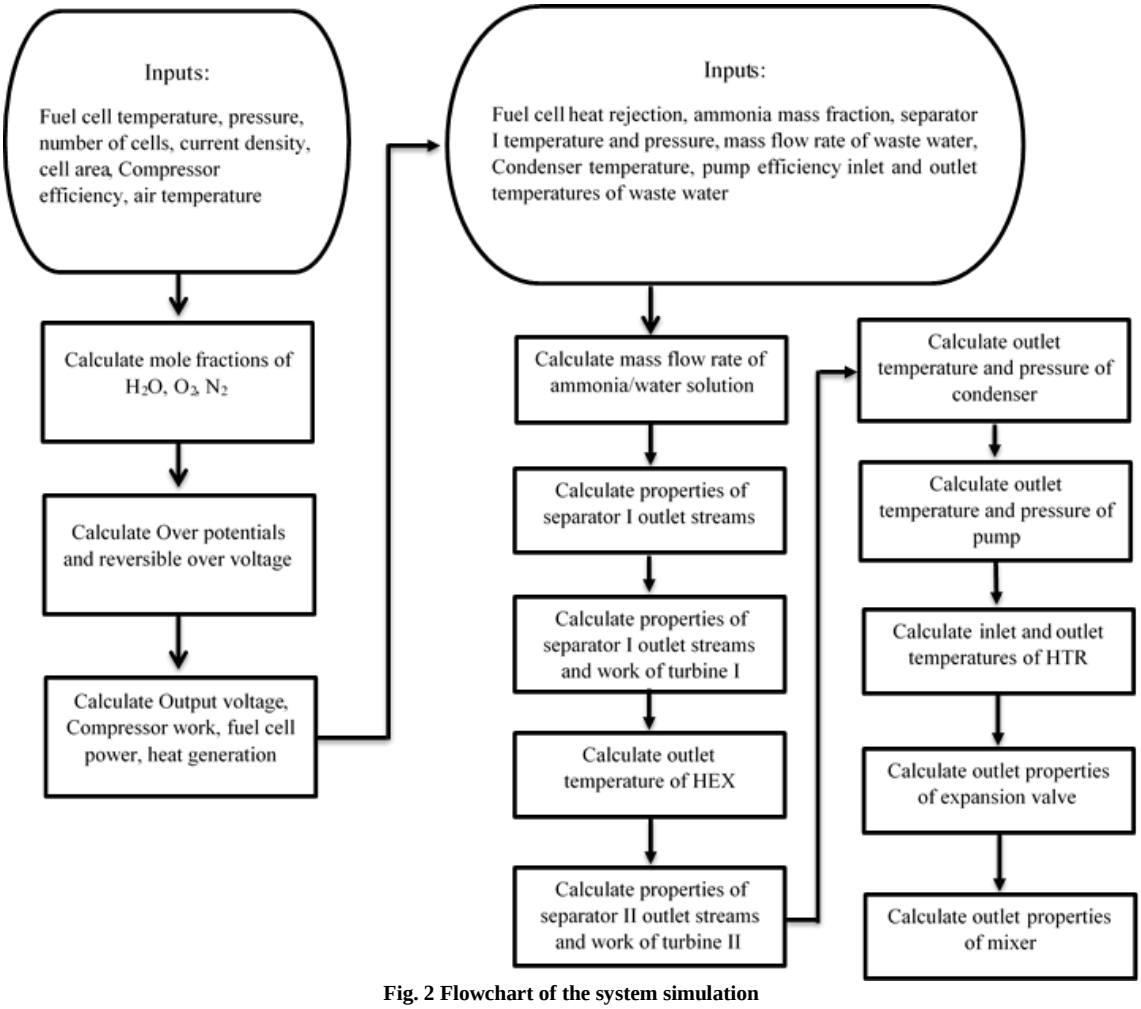

Fig. 2 Flowchart of the system simulation

The energy efficiency of the Kalina cycle which is defined as the ratio of the net power production of the Kalina cycle to the net input heat can be calculated as:

$$\eta_{Kalina} = \frac{\dot{W}_{turbine} - \dot{W}_{pump}}{\dot{Q}_{net} + \dot{Q}_{HEX}} \quad (39)$$

The overall energy efficiency of the proposed system can be obtained as follows:

$$\eta_{Overall} = \frac{\dot{W}_{fc} + \dot{W}_{turbine} - \dot{W}_{pump} - \dot{W}_{comp}}{\left(\dot{n}_{H_2,cons}\right).HHV + \dot{Q}_{HEX}} \tag{40}$$

5. Exergy analysis

To determine a more precise thermodynamic evaluation, the second law of thermodynamics should be performed for all components of the system. Exergy is expressed as the maximum useful work obtained by a system when it reaches to equilibrium with environment. In order to apply exergy analysis on a system, the exergy balance equation is employed as follows:

$$\sum \dot{Q}_k \left(1 - \frac{T_0}{T_k}\right) + \sum \dot{m}_i ex_i = \sum \dot{m}_e ex_e + \sum \dot{W} + \dot{E}x_{D,k} \tag{41}$$

The first term in left side of the Eq. (37) is the exergy rate related to the heat transfer, ex_i and ex_o are the inlet and outlet specific exergy, respectively and $\dot{E}x_{D,k}$ represents the exergy destruction rate. The specific exergy is obtained from summation of the physical and chemical exergy [41].

$$ex = ex_{ph} + ex_{ch} \tag{42}$$

The physical exergy of a stream is defined as [41]:

$$ex_{ph} = \left(h - h_0\right) - T_0\left(s - s_0\right) \tag{43}$$

where h_0 and s_0 represent the specific enthalpy and specific entropy for ambient temperature, respectively. The chemical exergy is calculated using the following equation [52]:

$$ex_{ch} = \sum x_n ex_{ch,n} + RT_0 \sum x_n \ln x_n \tag{44}$$

where x_n is the mole fraction of species n and $ex_{ch,n}$ is the chemical exergy of the species n in dead state. In the Kalina cycle, due to changing the ammonia concentration in different points of the cycle, the chemical exergy can be calculated as follow [58]:

$$e_{ch} = \left[\frac{e^0_{ch,NH_3}}{M_{NH_3}}\right] y + \left[\frac{e^0_{ch,H_2O}}{M_{H_2O}}\right](1 - y) \tag{45}$$

where e^0_{ch,NH_3} and e^0_{ch,H_2O} are standard chemical exergy for ammonia and water, respectively. Moreover, M_{NH_3} and M_{H_2O} are the molecular weight of ammonia and molecular weight of water, respectively. Furthermore, y is the mass fraction of ammonia. The standard chemical exergies are taken from [59] .

Exergy efficiency for a system is defined as the product exergy to fuel exergy. The exergy efficiency for the Kalina cycle, PEM fuel cell and the overall system can be obtained from Eq. (46-48) respectively.

$$\eta_{II,Kalina} = \frac{\dot{W}_{turbine} - \dot{W}_{pump}}{\dot{Q}_{net}\left(1 - \frac{T_0}{T_{fc}}\right) + \dot{E}x_{15} - \dot{E}x_{16}} \tag{46}$$

$$\eta_{II,fc} = \frac{\dot{W}_{fc} - \dot{W}_{comp}}{\left(\dot{E}x_{air,in} + \dot{E}x_{H_2,in}\right) - \left(\dot{E}x_{air,out} + \dot{E}x_{H_2O,gen}\right)} \tag{47}$$

$$\eta_{II,Overall} = \frac{\dot{W}_{fc} - \dot{W}_{comp} + \dot{W}_{turbine} - \dot{W}_{pump}}{\left(\dot{E}x_{air,in} + \dot{E}x_{H_2,in}\right) - \left(\dot{E}x_{air,out} + \dot{E}x_{H_2O,gen}\right) + \dot{Q}_{HEX}\left(1 - \frac{T_0}{T_w}\right)} \tag{48}$$

6. Exergoeconomic analysis

Economic analysis is a decisive and crucial factor for determining the overall performance of thermodynamic systems. In this regards, the major costs of the system including the fuel cost, operating and maintenance costs and investment costs need to be evaluated. The cost balance equation for each component of the system can be written as [60]:

$$\sum \dot{C}_{out,k} + \dot{C}_w = \sum \dot{C}_{in,k} + \dot{C}_Q + \dot{Z}_k \tag{49}$$

$$\dot{C} = c\dot{E}x \tag{50}$$

Where $\dot{C}_{in,k}$ and $\dot{C}_{out,k}$ indicate the cost rates for the inlet and outlet of each component, respectively, and c is the cost rate per unit of exergy. The terms $\dot{C}_w$ and $\dot{C}_Q$ are the cost rates associated with the power and thermal energy for each component. $\dot{Z}_k$ is the summation of the investment and operation and maintenance cost rates for k_{th} component and can be obtained from Eq. (51) [52].

$$\dot{Z}_k = \frac{Z_k CRF\,\varphi}{N} \tag{51}$$

Where Z_k for each component is given in Table 1. Moreover, φ and N are the maintenance factor and the number of operating hours per year for the system, respectively. CRF indicates the capital recovery factor for the system and can be calculated as [52]:

$$CRF = \frac{i_r\left(1+i_r\right)^n}{\left(1+i_r\right)^n - 1} \tag{52}$$

where n is the lifetime and i_r is the discount rate. The levelized cost of energy is the system's investment and maintenance costs in its lifetime to the total net power output generated by the ORC system. It is used to carry out the total cost of the system on the output energies [61]. The LCOE can be calculated as:

$$LCOE = \frac{\dot{Z}_k}{\dot{W}_{net}} \tag{53}$$

Table 1: Cost functions for the system components

Component	Cost function ($)
Turbine [42]	$4750\left(\dot{W}_{tur}\right)^{0.75}$
Pump [42]	$3500\left(\dot{W}_{Pump}\right)^{0.41}$
Fuel cell [41]	$2500\left(\dot{W}_{FC}\right)$
HTR,HXE,Condenser [42]	$309.14\left(A_{Cond}\right)^{0.85}$
Separator [41]	$280.3\left(\dot{m}_{Seperator-inlet}\right)^{0.67}$
Compressor [45]	$\left(\frac{0.75\dot{m}_{air}}{0.9-\eta_{comp}}\right)\left(\frac{P_{out}}{P_{in}}\right)\ln\left(\frac{P_{out}}{P_{in}}\right)$

The cost rates associated with the fuel, products and exergy destruction can be expressed as [41]:

$$c_{P,k} = \frac{\dot{C}_{P,k}}{\dot{E}x_{P,k}} \tag{54}$$

$$c_{F,k} = \frac{\dot{C}_{F,k}}{\dot{E}x_{F,k}} \tag{55}$$

$$\dot{C}_{D,k} = c_{F,k}\dot{E}x_{D,k} \tag{56}$$

where, $\dot{C}_{F,k}$ and $\dot{C}_{P,k}$ are specific cost rate of fuel and products exergy for the k_{th} component, respectively. The cost related to each component can be divide into exergetic costs and non-exergetic costs (investment and operation and maintenance costs). It is important to distinguish which cost is more dominant. The exergoeconomic factor indicates the contribution of non-exergetic costs to the total cost of each component can be obtained from Eq. (57) [41].

$$f_k = \frac{\dot{Z}_k}{\dot{Z}_k + \dot{C}_{D,k}} \tag{57}$$

Consequently, the overall exergoeconomic factor can be written as [52]:

$$f_{overall} = \frac{\dot{Z}_{overall}}{\dot{Z}_{overall} + \dot{C}_{D,overall}} \tag{58}$$

7. Results and Discussion

The input parameters used in the present study are shown in Table 2. The EES software is employed to perform thermodynamic modeling of the proposed system.

Table 2: The input parameters of the system

Parameter	Value	Parameter	Value
Farady Constant [48]	96485 (C/mol)	Turbine isentropic efficiency [48]	85%
Number of electrons [48]	2	Pump isentropic efficiency [48]	70%
Number of cells [48]	13000	Compressor isentropic efficiency [48]	85%
Limiting current density [44]	1.5 (A/ cm^2)	Mass flow rate of heat source [62]	4.977 (kg/s)
Stack operating current density [44]	0.6 (A/ cm^2)	Temperature of inlet waste water [62]	373 (K)
Active surface area [48]	232 (cm^2)	Pressure of waste water [62]	1 (bar)
Membrane thickness [44]	0.0178 (cm)	Temperature of outlet waste water[62]	358 (K)
Operating temperature of PEM [48]	358.15 (K)	Turbine inlet pressure	34 (bar)
Operating pressure of PEM [48]	3 (bar)	Concentration of basic solution	0.9
Stoichiometric rate of hydrogen [52]	1.2	Temperature difference in HTR [58]	5 (K)
Stoichiometric rate of air [52]	2	Ambient temperature	293.15 (K)
Vaporization heat of water [48]	40644 J/mol	Ambient pressure	1 (bar)
Specific heat capacity of oxygen [48]	29.72 J/(mol.K)	Maintenance factor [41]	1.06
Specific heat capacity of nitrogen [48]	28.39 J/(mol.K)	Discount rate [41]	12 %
Specific heat capacity of hydrogen [48]	28.86 J/(mol.K)	System lifetime [41]	15 (years)
Specific heat capacity of water [48]	75.95 J/(mol.K)	Operating hours per year [52]	7300
Higher heating value of hydrogen [48]	285.55 J/(mol.K)	Cost of the hydrogen [45]	10 ($/GJ)
Condenser cooling water input temperature	25 (°C)	Turbine isentropic efficiency [48]	85%
Farady Constant [48]	96485 (C/mol)		

In order to validate the calculations of the Kalina cycle, the data reported in Ref [58] is used for thermodynamic modeling. Regarding Table 3, good agreements can be observed between the simulated results with those reported by Fallah et al [58]. Furthermore, the verification for the PEM fuel cell modeling results, is performed by comparing the cell voltage and single sell output power variations versus current density with those presented by Ahmadi et al [44]. As it can be observed form Fig. 3 the results obtained in this study can reach an acceptable agreement with data in Ref [44].

Table 3: Comparison of Kalina cycle parameters with Ref [58]

Parameter	Present model results (kW))	Ref [58] model results (kW)	Error (%)
$\dot{W}_{turbine}$	1827	1820	0.38
$\dot{W}_{Pump}$	92.24	93.72	1.6
η_{th}	0.0645	0.06241	3.2

η_{II}	0.3845	0.3787	1.5

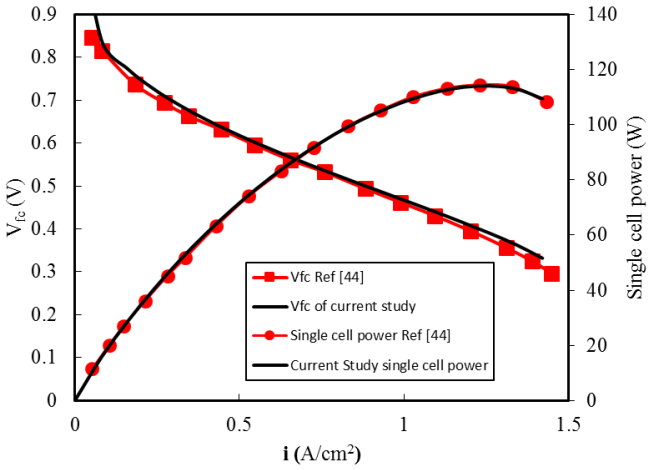

Fig. 3. Fuel cell modeling verification by [44]

The energy and exergy related parameters of the proposed system is presented in Table 4. As can be observed, the output power of the PEM fuel cell is 1058 kW. Moreover, 153.61 kW power can be obtained from the proposed Kalina cycle by recovering the waste heat of the PEM fuel cell. Hence, the proposed hybrid system can produce 14.51% more power in comparison with the stand alone PEM fuel cell. Furthermore, the energy efficiency and exergy efficiency of the proposed hybrid system are improved by 5.01 % and 14%, respectively in comparison with the stand alone PEM fuel cell.

Table 4: Energy and exergy parameters of the proposed system

Parameter	Value
$\dot{W}_{turbineI}$ (kW)	122.1
$\dot{W}_{turbineII}$ (kW)	41.85
$\dot{W}_{Pump}$ (kW)	10.34
η_{Kalina} (%)	10.12
$\eta_{II,Kalina}$ (%)	54.72
$\dot{W}_{fc}$ (kW)	1058
$\dot{Q}_{net}$ (kW)	1204
$\dot{W}_{comp}$ (kW)	175.4
η_{fc} (%)	32.96
$\eta_{II,fc}$ (%)	41.77
η_{total} (%)	34.64
$\eta_{II,total}$ (%)	47.65

The values of some important exergy and exergoeconomic factors for evaluating the system performance including exergy destruction rate, exergy destruction cost rate, investment and operation and maintenance cost rate, the sum of the exergy destruction cost rate and investment and operation and maintenance cost rate, exergoeconomic factor, and relative cost difference are presented in Table 5. As can be seen form Table 5, the fuel cell, the turbines,

the compressor and the condenser have the highest value of $\dot{Z}_k+\dot{C}_{D,k}$. However, the value of $\dot{Z}_k+\dot{C}_{D,k}$ is more considerable for the PEM. The value of $\dot{Z}_k+\dot{C}_{D,k}$ for the proposed hybrid system is 131 ($/h) which is 19.3% higher than the total cost rate of the stand-alone PEM fuel cell. The turbines, the PEM fuel cell and the condenser have a relatively high exergoeconomic factor compared to other components of the system. Hence, the investment costs are more important for these components. Furthermore, the values of exergoeconomic factor for the HTR, HEX and the separators is below 50% and, therefore, the cost related to exergy destruction for these components is higher than the investment and operation and maintenance cost. Accordingly, design of these components needs to be improved. The overall exergoeconomic factor for the system is 55.52 %. Thus, the exergy destruction accounts for 44.48 % of the total cost rate of the system.

Table 5: Exergoeconomic results for the proposed system.

Parameters	$\dot{E}_{D,k}$ (kW)	$\dot{Z}_k$ ($/h)	$\dot{C}_{D,k}$ ($/h)	$\dot{Z}_k+\dot{C}_{D,k}$ ($/h)	f_k (%)
Turbine I	21.1	4.126	1.871	5.997	68.8
Turbine II	7.29	1.848	0.647	2.495	74.06
HEX	7.06	0.4964	0.555	1.051	47.21
HTR	13.76	0.621	1.22	1.841	33.73
Fuel cell	926.505	62.52	47.29	109.8	56.94
Condenser	24.21	2.715	2.147	4.862	55.84
Separator I	0.69	0.01094	0.06143	0.0723	15.12
Separator II	0.16	0.0076	0.01424	0.02184	34.78
Pump	2.05	0.2095	0.2131	0.4226	49.57
Compressor	38.16	0.1513	3.968	4.1193	3.67
Trottling valve	3.12	-	0.2772	0.2772	-
Overall system	1044.105	72.705	58.263	130.959	55.52

The effect of current density on energy efficiency, exergy efficiency and total cost rates are shown in Fig. 4a and b. As can be observed from Fig. 4a by increasing the current density, the fuel cell power and heat rejected from the fuel cell increase. In higher current densities, the voltage losses increase which leads to increase the heat generation in the fuel cell. Therefore, more energy is delivered to the Kalina cycle. Besides, due to the constant operating temperature of the fuel cell, the maximum temperature of the Kalina cycle also remains constant. Hence, the mass flow rate of the ammonia/water and the power of the Kalins cycle increase. However, for current density values below 1.3, increasing the voltage losses and subsequently decreasing the voltage of the fuel cell cannot compensate for the increase in current density. Accordingly, the fuel cell power increases with increasing the current density. As san be observed from Fig. 4a the fuel cell efficiency decreases with increasing the current density. In higher current densities the hydrogen molar flow rate to the fuel cell increases which leads to decrease the energy and exergy efficiencies of the fuel cell. Although the power produced by the Kalina cycle increases in higher current densities, but the overall efficiency of the system decreases. By increasing the current density and subsequently increasing the irreversibilities like voltage losses, the exergy destruction cost rates increase .Moreover, increasing the output power of the Kalina turbines and fuel cell, increase the total cost rates of the system.

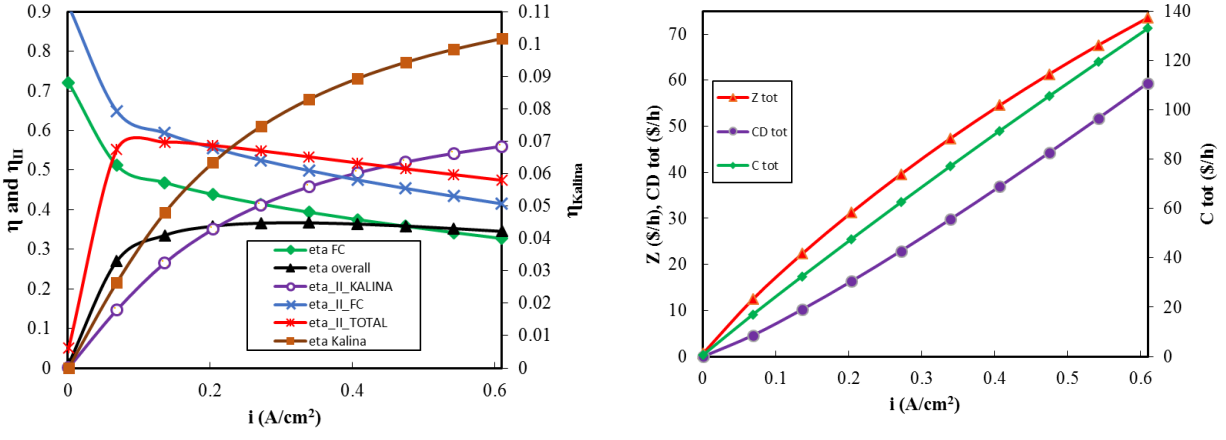

(a) **(b)**

Fig. 4. Effect of Variations of current density on a) energy and exergy efficiency, b) total cost rates.

The variations of thermodynamic and economic parameters of the system with fuel cell temperature are shown in Fig. 5a and b. In higher temperatures better ion exchange takes place in the fuel cell and cell voltage increases. Therefore, the fuel cell power increases with increasing the fuel cell temperature. On the other hand, due to reduction in voltage losses, the waste heat of the fuel cell decreases. Hence, the energy and exergy efficiencies of the fuel cell increase with increasing the operating temperature. Accordingly, less energy is delivered to the Kalina cycle and the power generation of the turbines decreases. Although the fuel cell power increases with increasing the fuel cell temperature, but the reduction in the Kalina cycle power is more dominant and the overall energy and exergy of the system decrease. Furthermore, with increasing the operating temperature of the fuel cell, the maximum temperature of the Kalina cycle increases. Hence, the quality of the ammonia/water entering separator I increases and consequently the quality of the stream entering separator II decreases. On the other hand, decreasing the heat delivery to the Kalina cycle decrease the mass flow rate of the ammonia/water. Therefore, the power of turbine I increases and the power of turbine II decreases. However, the net power of the system decreases which leads to a reduction in the energy and exergy efficiencies of the system. As can be observed from Fig. 5b, increasing fuel cell operating temperature, leads to a reduction in the unit cost of the Kalina cycle output power. However, the unit cost rate of the fuel cell output power almost remains constant. Therefore, a slight decrease in total system cost rate can be observed with increasing the fuel cell operating temperature.

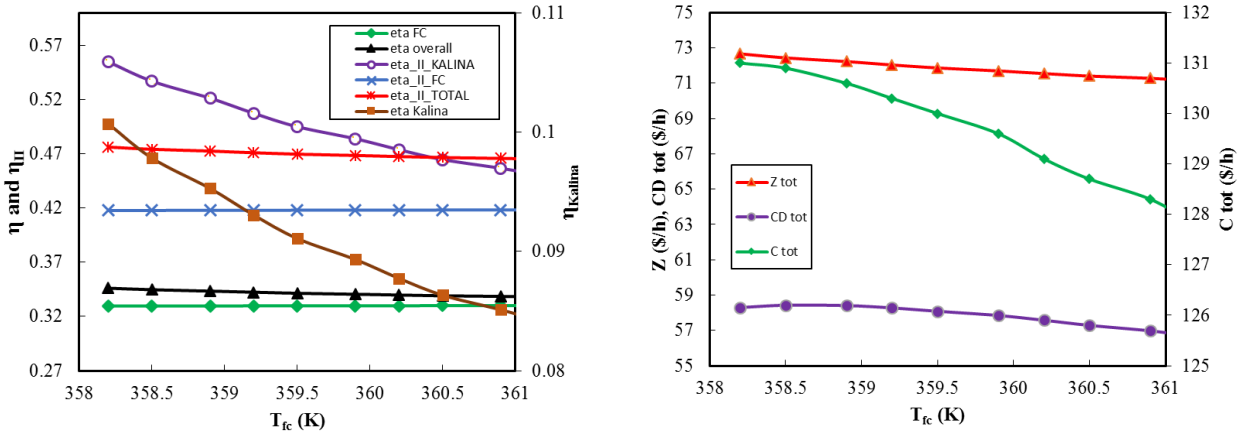

(a) **(b)**

Fig. 5. Effect of Variations of fuel cell operating temperature on a) energy and exergy efficiency, b) total cost rates.

Fig. 6a and b show the effect of fuel cell operating pressure on energy efficiency, exergy efficiency and total cost rates of the system. As can be observed from Fig.6a, by increasing the fuel cell operation pressure, the energy and exergy efficiencies of the system increase. The reason is that increasing the fuel cell operating pressure can improve the diffusivity of the reactant gases and the over potentials of the fuel cell decrease. Therefore, the cell voltage and consequently the power of the fuel cell increase. On the other hand, by enhancing the cell performance, the heat generation of the fuel cell decreases. Hence, delivered energy to the Kalina cycle, the work of the turbines and the energy efficiency of the Kalina cycle decrease. However, the net efficiency of the system enhances. By increasing the fuel cell power and decreasing the Kalina turbines work, the operating and maintenance costs increase and exergy destructions of the system decrease.

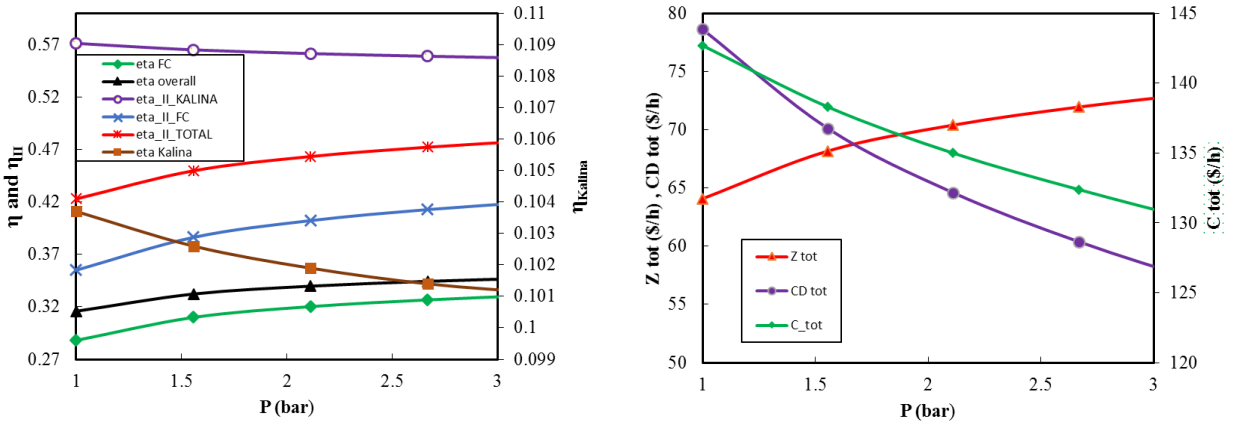

(a) (b)

Fig. 6. Effect of Variations of fuel cell operating Pressure on a) energy and exergy efficiency, b) total cost rates.

Fig. 7a and b depict the effect of pressure in separator I on thermodynamic and thermo economic performance of the system. According to the Fig. 7a, by increasing the pressure of separator I, the total produced work of the Kalina cycle increases. With increasing the pressure of separator I, the enthalpy difference in turbine I increases, whereas the mass flow rate of rich ammonia vapor outlet of the separator I decreases. Hence the work produced by the turbine I firstly increases then decreases. On the other hand, by increasing the mass flow rate of poor ammonia/water outlet of the separator I, the produced work by turbine II increases. The increase in the power of turbine II is more prominent and the total power of the Kalina cycle increases. Therefore, the energy and exergy efficiencies of the Kalina cycle and total system increase with increasing the pressure in separator I. Referring to the Fig. 6b, in higher pressures of the separator I, the total cost rates of the system increase. However, the costs related to the exergy destruction of the system almost remain constant. Hence, in higher pressures of separator I, the operation and maintenance costs are the considerable costs of the system.

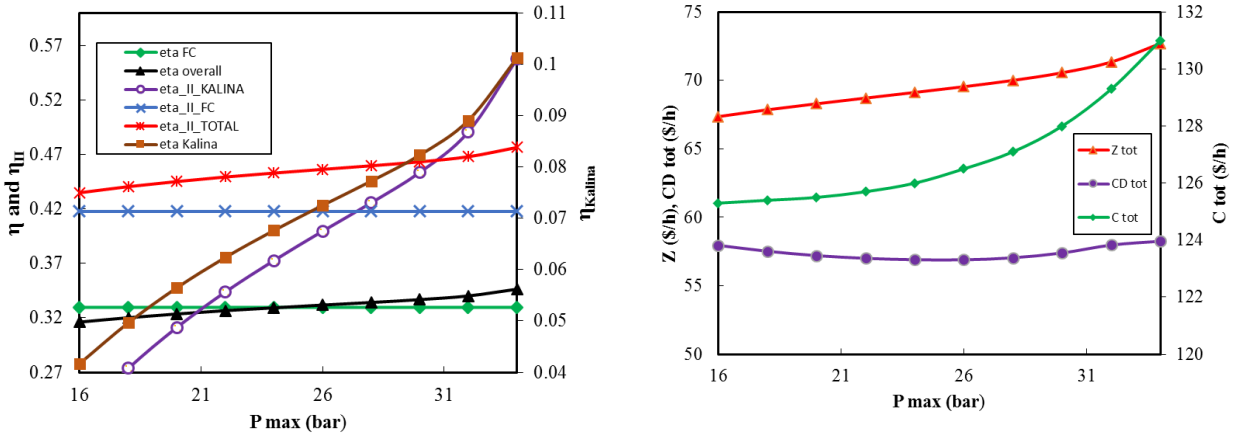

(a) (b)

Fig. 7. Effect of Variations of separator I pressure on a) energy and exergy efficiency, b) total cost rates.

The thermodynamic and economic behaviors of the system with variations of the ammonia mass fraction are shown in Fig. 8a and b. Increasing the ammonia mass fraction leads to an increase in the mass flow rate of ammonia rich vapor leaving the separator I. Consequently, the mass flow rate of ammonia/water poor solution entering the separator II, decreases. However, the enthalpy difference through the turbines remain constant. Therefore, the power generation of turbine I increases and the power generation of turbine II decreases with increasing the mass fraction of ammonia. Accordingly, the total power generation of the Kalina cycle and energy efficiency of the system decrease. Furthermore, in lower mass fraction of the stream entering the HEX, the exergy destruction in HEX increases which is the most considerable factor for increasing the exergy destruction in the Kalina cycle. Reduction in total work of the Kalina cycle along with increasing the exergy destruction reduce the exergy efficiency of the system. As can be observed from Fig.8b with increasing the ammonia mass fraction the operation and maintenance

cost rates and the exergy destruction cost rates decrease. Furthermore, variations of the ammonia mass fraction dos not affect the cost rates of the fuel cell. However, with increasing the ammonia mass fraction, the total cost rates of the system decrease.

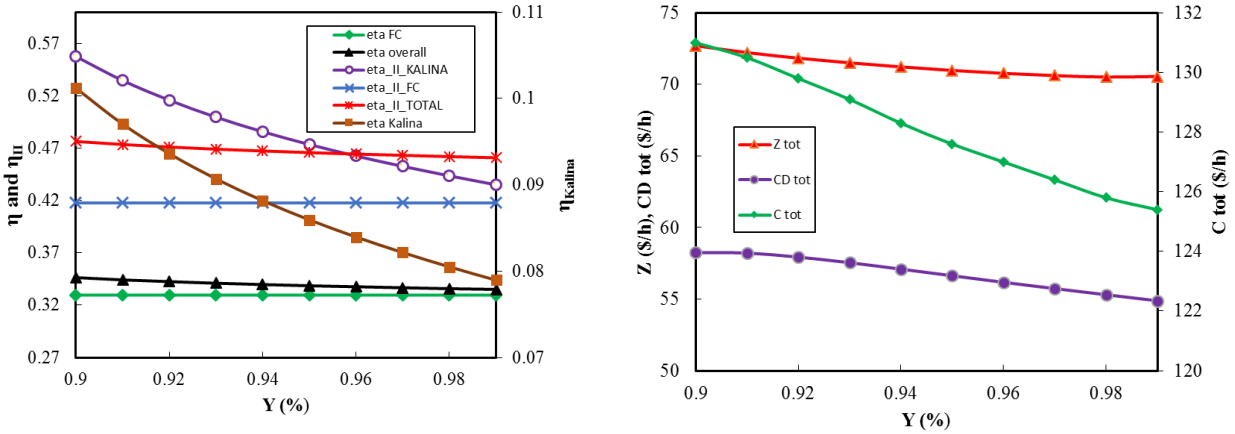

(a) **(b)**

Fig. 8. Effect of Variations of ammonia mass fraction on a) energy and exergy efficiency, b) total cost rates.

A sensitivity analysis is performed by system investment parameters to see how levelized cost of energy is sensitive to the variations of PEM fuel cell costs, Kalina cycle costs, and discount rate. As displayed in Fig. 9, based on the sensitivity analysis results, it can be observed that the costs of the PEM fuel cell have most impact on the LOCE while the Kalina cycle costs rate and discount rate are the least influencing parameters.

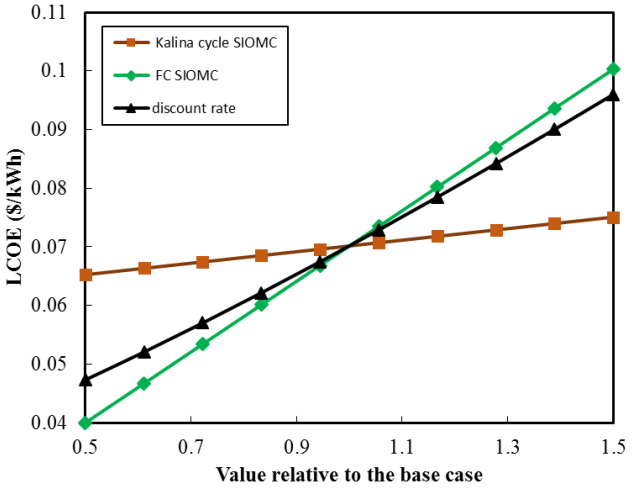

Fig. 9. sensitivity analysis results for system investment parameters

8. Conclusion

In this research, recovering the waste heat rejected from a proton exchange membrane fuel cell is investigated. For this purpose, an improved Kalina cycle has been proposed. The waste heat of PEM fuel cell is the main energy source for the system. Moreover, the energy of weak ammonia/water solution leaving the separator of the Kalina cycle is improved by industrial waste heat to produce more electrical energy through the second turbine placed in the Kalina cycle. Thermodynamic and thermo economic analysis is performed on the system. Moreover, the effect of some key parameters on thermodynamic and exergoeconomic performance of the system is investigated.

The important results of this study can be summarized as follows:

- The energy and exergy efficiencies of the proposed hybrid system are 5.01 % and 14 % higher than the energy and exergy efficiencies of the standalone PEM fuel cell.
- Increasing the current density of the PEM fuel cell increases the power and the rejected heat from the fuel cell as well as the Kalina cycle power. However, overall energy and exergy efficiencies of the system

decrease with increasing the current density. Furthermore, the total cost rates of the system increase in higher current densities of the fuel cell.

- Increasing the fuel cell operating temperature leads to an increase in the fuel cell output power. However, the waste heat of the fuel cell decreases which result in decrease the Kalina power generation and overall energy and exergy of the system. Moreover, a slight decrease is observed in the total cost rates of the system with increasing the fuel cell operating temperature.
- Increasing the fuel cell operating pressure increases the overall energy and exergy efficiencies of the system. Moreover, the total cost rates of the system decrease with increasing the operating pressure of the fuel cell.
- By increasing the ammonia mass fraction, the energy efficiency, exergy efficiency and the overall cost rates of the system decrease.
- By increasing the pressure in separator I, total power generation of the system, energy efficiency, exergy efficiency, and the total cost rates of the system increase.

Nomenclature

C_p	Specific heat capacity (J/mol-K)	Greek letters	
c	Cost per unit exergy ($/GJ)	η	Energy efficiency
$\dot{C}$	Cost rate ($/h)	η_{II}	Exergy efficiency
CRF	Capital recovery factor	λ	Stoichiometric ratio
cond	Condenser	ψ	Membrane hydration
cw	Cooling water	N	Annual plant operation hours
$\dot{E}x$	Exergy rate (kW)	Subscripts	
ex	Specific exergy (kJ/kg)	act	Activation
F	Faraday constant (C/mol)	comp	Compressor
f	Exergoeconomic factor	conc	Concentration
h	Specific enthalpy (kJ/kg)	D	Destruction
HHV	High heating value J/(mol.K)	fc	Fuel cell
HTR	high-temperature recuperator	H_2	Hydrogen
HEX	Heat exchanger	H_2O	Water
I	Current (A)	N_2	Nitrogen
i	Current density (A/cm2)	O_2	Oxygen
i_L	Limiting current density (A/cm2)	ph	Physical
L	Membrane thickness (cm)	sat	Saturation
LCOE	Levelized cost of energy	tur	Turbine
$\dot{m}$	Mass flow rate (kg/s)		
N	Annual plant operation hours (h)		
N_{cell}	Number of cells		
n_e	Number of electrons		
P	Pressure (bar)		
PEM	Proton exchange membrane		
r_{mem}	Membrane resistivity		
SIOMC	sum of the investment and operation and maintenance cost		
T	Temperature (K)		
V	Voltage (V)		
$\dot{Z}$	Cost rate of components ($/h)		

References

[1] A. Çalık, S. Yıldırım, E. Tosun, Estimation of crack propagation in polymer electrolyte membrane fuel cell under vibration conditions, *International Journal of Hydrogen Energy*, Vol. 42, No. 36, pp. 23347-23351, 2017/09/07/, 2017.

[2] H. Serin, Ş. Yıldızhan, Hydrogen addition to tea seed oil biodiesel: Performance and emission characteristics, *International Journal of Hydrogen Energy*, Vol. 43, No. 38, pp. 18020-18027, 2018/09/20/, 2018.

[3] G. Tüccar, E. Uludamar, Emission and engine performance analysis of a diesel engine using hydrogen enriched pomegranate seed oil biodiesel, *International Journal of Hydrogen Energy*, Vol. 43, No. 38, pp. 18014-18019, 2018/09/20/, 2018.

[4] Y. Wang, D. F. Ruiz Diaz, K. S. Chen, Z. Wang, X. C. Adroher, Materials, technological status, and fundamentals of PEM fuel cells – A review, *Materials Today*, Vol. 32, pp. 178-203, 2020/01/01/, 2020.

[5] H. Asemi, S. Asemi, A. Farajpour, M. Mohammadi, Nanoscale mass detection based on vibrating piezoelectric ultrathin films under thermo-electro-mechanical loads, *Physica E: Low-dimensional Systems and Nanostructures*, Vol. 68, pp. 112-122, 2015.

[6] S. Asemi, A. Farajpour, H. Asemi, M. Mohammadi, Influence of initial stress on the vibration of double-piezoelectric-nanoplate systems with various boundary conditions using DQM, *Physica E: Low-dimensional Systems and Nanostructures*, Vol. 63, pp. 169-179, 2014.

[7] S. Asemi, A. Farajpour, M. Mohammadi, Nonlinear vibration analysis of piezoelectric nanoelectromechanical resonators based on nonlocal elasticity theory, *Composite Structures*, Vol. 116, pp. 703-712, 2014.

[8] S. R. Asemi, M. Mohammadi, A. Farajpour, A study on the nonlinear stability of orthotropic single-layered graphene sheet based on nonlocal elasticity theory, *Latin American Journal of Solids and Structures*, Vol. 11, No. 9, pp. 1515-1540, 2014.

[9] M. Baghani, M. Mohammadi, A. Farajpour, Dynamic and Stability Analysis of the Rotating Nanobeam in a Nonuniform Magnetic Field Considering the Surface Energy, *International Journal of Applied Mechanics*, Vol. 08, No. 04, pp. 1650048, 2016.

[10] M. Danesh, A. Farajpour, M. Mohammadi, Axial vibration analysis of a tapered nanorod based on nonlocal elasticity theory and differential quadrature method, *Mechanics Research Communications*, Vol. 39, No. 1, pp. 23-27, 2012.

[11] A. Farajpour, M. Danesh, M. Mohammadi, Buckling analysis of variable thickness nanoplates using nonlocal continuum mechanics, *Physica E: Low-dimensional Systems and Nanostructures*, Vol. 44, No. 3, pp. 719-727, 2011.

[12] A. Farajpour, M. Mohammadi, A. Shahidi, M. Mahzoon, Axisymmetric buckling of the circular graphene sheets with the nonlocal continuum plate model, *Physica E: Low-dimensional Systems and Nanostructures*, Vol. 43, No. 10, pp. 1820-1825, 2011.

[13] A. Farajpour, A. Rastgoo, M. Mohammadi, Surface effects on the mechanical characteristics of microtubule networks in living cells, *Mechanics Research Communications*, Vol. 57, pp. 18-26, 2014.

[14] A. Farajpour, A. Rastgoo, M. Mohammadi, Vibration, buckling and smart control of microtubules using piezoelectric nanoshells under electric voltage in thermal environment, *Physica B: Condensed Matter*, Vol. 509, pp. 100-114, 2017.

[15] A. Farajpour, A. Shahidi, M. Mohammadi, M. Mahzoon, Buckling of orthotropic micro/nanoscale plates under linearly varying in-plane load via nonlocal continuum mechanics, *Composite Structures*, Vol. 94, No. 5, pp. 1605-1615, 2012.

[16] A. Farajpour, M. Yazdi, A. Rastgoo, M. Mohammadi, A higher-order nonlocal strain gradient plate model for buckling of orthotropic nanoplates in thermal environment, *Acta Mechanica*, Vol. 227, No. 7, pp. 1849-1867, 2016.

[17] A. Farajpour, M. H. Yazdi, A. Rastgoo, M. Loghmani, M. Mohammadi, Nonlocal nonlinear plate model for large amplitude vibration of magneto-electro-elastic nanoplates, *Composite Structures*, Vol. 140, pp. 323-336, 2016.

[18] M. R. Farajpour, A. Rastgoo, A. Farajpour, M. Mohammadi, Vibration of piezoelectric nanofilm-based electromechanical sensors via higher-order non-local strain gradient theory, *Micro & Nano Letters*, Vol. 11, No. 6, pp. 302-307, 2016.

[19] N. GHAYOUR, A. SEDAGHAT, M. MOHAMMADI, WAVE PROPAGATION APPROACH TO FLUID FILLED SUBMERGED VISCO-ELASTIC FINITE CYLINDRICAL SHELLS, *JOURNAL OF AEROSPACE SCIENCE AND TECHNOLOGY (JAST)*, Vol. 8, No. 1, pp. -, 2011.

[20] M. GOODARZI, M. MOHAMMADI, A. FARAJPOUR, M. KHOORAN, INVESTIGATION OF THE EFFECT OF PRE-STRESSED ON VIBRATION FREQUENCY OF RECTANGULAR NANOPLATE BASED ON A VISCO-PASTERNAK FOUNDATION, *JOURNAL OF SOLID MECHANICS*, Vol. 6, No. 1, pp. -, 2014.

[21] M. Goodarzi, M. Mohammadi, M. Khooran, F. Saadi, Thermo-Mechanical Vibration Analysis of FG Circular and Annular Nanoplate Based on the Visco-Pasternak Foundation, *Journal of Solid Mechanics*, Vol. 8, No. 4, pp. 788-805, 2016.

[22] M. Mohammadi, A. Farajpour, M. Goodarzi, F. Dinari, Thermo-mechanical vibration analysis of annular and circular graphene sheet embedded in an elastic medium, *Latin American Journal of Solids and Structures*, Vol. 11, pp. 659-682, 2014.

[23] M. Mohammadi, A. Farajpour, M. Goodarzi, R. Heydarshenas, Levy type solution for nonlocal thermo-mechanical vibration of orthotropic mono-layer graphene sheet embedded in an elastic medium, *Journal of Solid Mechanics*, Vol. 5, No. 2, pp. 116-132, 2013.

[24] M. Mohammadi, A. Farajpour, M. Goodarzi, H. Mohammadi, Temperature Effect on Vibration Analysis of Annular Graphene Sheet Embedded on Visco-Pasternak Foundati, *Journal of Solid Mechanics*, Vol. 5, No. 3, pp. 305-323, 2013.

[25] M. Mohammadi, A. Farajpour, M. Goodarzi, H. Shehni nezhad pour, Numerical study of the effect of shear in-plane load on the vibration analysis of graphene sheet embedded in an elastic medium, *Computational Materials Science*, Vol. 82, pp. 510-520, 2014/02/01/, 2014.

[26] M. Mohammadi, A. Farajpour, A. Moradi, M. Ghayour, Shear buckling of orthotropic rectangular graphene sheet embedded in an elastic medium in thermal environment, *Composites Part B: Engineering*, Vol. 56, pp. 629-637, 2014.

[27] M. Mohammadi, M. Ghayour, A. Farajpour, Analysis of Free Vibration Sector Plate Based on Elastic Medium by using New Version of Differential Quadrature Method, *Journal of Simulation and Analysis of Novel Technologies in Mechanical Engineering*, Vol. 3, No. 2, pp. 47-56, 2010.

[28] M. Mohammadi, M. Ghayour, A. Farajpour, Free transverse vibration analysis of circular and annular graphene sheets with various boundary conditions using the nonlocal continuum plate model, *Composites Part B: Engineering*, Vol. 45, No. 1, pp. 32-42, 2013.

[29] M. MOHAMMADI, M. GOODARZI, M. GHAYOUR, S. ALIVAND, SMALL SCALE EFFECT ON THE VIBRATION OF ORTHOTROPIC PLATES EMBEDDED IN AN ELASTIC MEDIUM AND UNDER BIAXIAL IN-PLANE PRE-LOAD VIA NONLOCAL ELASTICITY THEORY, *JOURNAL OF SOLID MECHANICS*, Vol. 4, No. 2, pp. -, 2012.

[30] M. Mohammadi, M. Goodarzi, M. Ghayour, A. Farajpour, Influence of in-plane pre-load on the vibration frequency of circular graphene sheet via nonlocal continuum theory, *Composites Part B: Engineering*, Vol. 51, pp. 121-129, 2013.

[31] M. Mohammadi, M. Hosseini, M. Shishesaz, A. Hadi, A. Rastgoo, Primary and secondary resonance analysis of porous functionally graded nanobeam resting on a nonlinear foundation subjected to mechanical and electrical loads, *European Journal of Mechanics - A/Solids*, Vol. 77, pp. 103793, 2019/09/01/, 2019.

[32] M. Mohammadi, A. Moradi, M. Ghayour, A. Farajpour, Exact solution for thermo-mechanical vibration of orthotropic mono-layer graphene sheet embedded in an elastic medium, *Latin American Journal of Solids and Structures*, Vol. 11, No. 3, pp. 437-458, 2014.

[33] M. Mohammadi, A. Rastgoo, Nonlinear vibration analysis of the viscoelastic composite nanoplate with three directionally imperfect porous FG core, *Structural Engineering and Mechanics, An Int'l Journal*, Vol. 69, No. 2, pp. 131-143, 2019.

[34] M. Mohammadi, A. Rastgoo, Primary and secondary resonance analysis of FG/lipid nanoplate with considering porosity distribution based on a nonlinear elastic medium, *Mechanics of Advanced Materials and Structures*, Vol. 27, No. 20, pp. 1709-1730, 2020.

[35] M. Mohammadi, M. Safarabadi, A. Rastgoo, A. Farajpour, Hygro-mechanical vibration analysis of a rotating viscoelastic nanobeam embedded in a visco-Pasternak elastic medium and in a nonlinear thermal environment, *Acta Mechanica*, Vol. 227, No. 8, pp. 2207-2232, 2016.

[36] H. Moosavi, M. Mohammadi, A. Farajpour, S. H. Shahidi, Vibration analysis of nanorings using nonlocal continuum mechanics and shear deformable ring theory, *Physica E: Low-dimensional Systems and Nanostructures*, Vol. 44, No. 1, pp. 135-140, 2011/10/01/, 2011.

[37] M. Safarabadi, M. Mohammadi, A. Farajpour, M. Goodarzi, Effect of surface energy on the vibration analysis of rotating nanobeam, 2015.

[38] M. Hasani, N. Rahbar, Application of thermoelectric cooler as a power generator in waste heat recovery from a PEM fuel cell – An experimental study, *International Journal of Hydrogen Energy*, Vol. 40, No. 43, pp. 15040-15051, 2015/11/16/, 2015.

[39] M. Ni, M. K. H. Leung, K. Sumathy, D. Y. C. Leung, Potential of renewable hydrogen production for energy supply in Hong Kong, *International Journal of Hydrogen Energy*, Vol. 31, No. 10, pp. 1401-1412, 2006/08/01/, 2006.

[40] H. Q. Nguyen, B. Shabani, Proton exchange membrane fuel cells heat recovery opportunities for combined heating/cooling and power applications, *Energy Conversion and Management*, Vol. 204, pp. 112328, 2020/01/15/, 2020.

[41] M. Z. Malik, F. Musharavati, S. Khanmohammadi, A. H. Pakseresht, S. Khanmohammadi, D. D. Nguyen, Design and comparative exergy and exergo-economic analyses of a novel integrated Kalina cycle improved with fuel cell and thermoelectric module, *Energy Conversion and Management*, Vol. 220, pp. 113081, 2020/09/15/, 2020.

[42] Z. Li, S. Khanmohammadi, S. Khanmohammadi, A. A. A. A. Al-Rashed, P. Ahmadi, M. Afrand, 3-E analysis and optimization of an organic rankine flash cycle integrated with a PEM fuel cell and geothermal energy, *International Journal of Hydrogen Energy*, Vol. 45, No. 3, pp. 2168-2185, 2020/01/13/, 2020.

[43] N. Sarabchi, S. M. S. Mahmoudi, M. Yari, A. Farzi, Exergoeconomic analysis and optimization of a novel hybrid cogeneration system: High-temperature proton exchange membrane fuel cell/Kalina cycle, driven by solar energy, *Energy Conversion and Management*, Vol. 190, pp. 14-33, 2019/06/15/, 2019.

[44] M. H. Ahmadi, A. Mohammadi, F. Pourfayaz, M. Mehrpooya, M. Bidi, A. Valero, S. Uson, Thermodynamic analysis and optimization of a waste heat recovery system for proton exchange membrane fuel cell using transcritical carbon dioxide cycle and cold energy of liquefied natural gas, *Journal of Natural Gas Science and Engineering*, Vol. 34, pp. 428-438, 2016/08/01/, 2016.

[45] S. M. Seyed Mahmoudi, N. Sarabchi, M. Yari, M. A. Rosen, Exergy and Exergoeconomic Analyses of a Combined Power Producing System including a Proton Exchange Membrane Fuel Cell and an Organic Rankine Cycle, *Sustainability*, Vol. 11, No. 12, 2019.

[46] V. Rezaee, A. Houshmand, Energy and Exergy Analysis of a Combined Power Generation System Using PEM Fuel Cell and Kalina Cycle System 11, *Periodica Polytechnica Chemical Engineering*, Vol. 60, pp. 98-105, 03/25, 2016.

[47] M. Chahartaghi, B. A. Kharkeshi, Performance analysis of a combined cooling, heating and power system with PEM fuel cell as a prime mover, *Applied Thermal Engineering*, Vol. 128, pp. 805-817, 2018/01/05/, 2018.

[48] P. Zhao, J. Wang, L. Gao, Y. Dai, Parametric analysis of a hybrid power system using organic Rankine cycle to recover waste heat from proton exchange membrane fuel cell, *International Journal of Hydrogen Energy*, Vol. 37, No. 4, pp. 3382-3391, 2012/02/01/, 2012.

[49] S. Kaushik A, S. S. Bhogilla, P. Muthukumar, Thermal integration of Proton Exchange Membrane Fuel Cell with recuperative organic rankine cycle, *International Journal of Hydrogen Energy*, Vol. 46, No. 27, pp. 14748-14756, 2021/04/19/, 2021.

[50] S. Toghyani, E. Afshari, E. Baniasadi, Performance evaluation of an integrated proton exchange membrane fuel cell system with ejector absorption refrigeration cycle, *Energy Conversion and Management*, Vol. 185, pp. 666-677, 2019/04/01/, 2019.

[51] E. Baniasadi, S. Toghyani, E. Afshari, Exergetic and exergoeconomic evaluation of a trigeneration system based on natural gas-PEM fuel cell, *International Journal of Hydrogen Energy*, Vol. 42, No. 8, pp. 5327-5339, 2017/02/23/, 2017.

[52] S. Marandi, F. Mohammadkhani, M. Yari, An efficient auxiliary power generation system for exploiting hydrogen boil-off gas (BOG) cold exergy based on PEM fuel cell and two-stage ORC: Thermodynamic and exergoeconomic viewpoints, *Energy Conversion and Management*, Vol. 195, pp. 502-518, 2019/09/01/, 2019.

[53] I. Fakhari, A. Behzadi, E. Gholamian, P. Ahmadi, A. Arabkoohsar, Comparative double and integer optimization of low-grade heat recovery from PEM fuel cells employing an organic Rankine cycle with zeotropic mixtures, *Energy Conversion and Management*, Vol. 228, pp. 113695, 2021/01/15/, 2021.

[54] M. D. Mirolli, Cementing Kalina cycle effectiveness, *IEEE Industry Applications Magazine*, Vol. 12, No. 4, pp. 60-64, 2006.

[55] M. D. Mirolli, 2007, *Ammonia-water based thermal conversion technology: Applications in waste heat recovery for the cement industry*,

[56] S. Ogriseck, Integration of Kalina cycle in a combined heat and power plant, a case study, *Applied Thermal Engineering*, Vol. 29, No. 14, pp. 2843-2848, 2009/10/01/, 2009.

[57] X. Zhang, M. He, Y. Zhang, A review of research on the Kalina cycle, *Renewable and Sustainable Energy Reviews*, Vol. 16, No. 7, pp. 5309-5318, 2012/09/01/, 2012.

[58] M. Fallah, S. M. S. Mahmoudi, M. Yari, R. Akbarpour Ghiasi, Advanced exergy analysis of the Kalina cycle applied for low temperature enhanced geothermal system, *Energy Conversion and Management*, Vol. 108, pp. 190-201, 2016/01/15/, 2016.

[59] J. Szargut, 2005, *Exergy Method: Technical and Ecological Applications*, WIT Press,

[60] V. Zare, S. M. S. Mahmoudi, M. Yari, On the exergoeconomic assessment of employing Kalina cycle for GT-MHR waste heat utilization, *Energy Conversion and Management,* Vol. 90, pp. 364-374, 2015/01/15/, 2015.

[61] R. Zhar, A. Allouhi, A. Jamil, K. Lahrech, A comparative study and sensitivity analysis of different ORC configurations for waste heat recovery, *Case Studies in Thermal Engineering,* Vol. 28, pp. 101608, 2021/12/01/, 2021.

[62] V. Jain, S. S. Kachhwaha, G. Sachdeva, Thermodynamic performance analysis of a vapor compression–absorption cascaded refrigeration system, *Energy Conversion and Management,* Vol. 75, pp. 685-700, 2013/11/01/, 2013.